



HAL
open science

Formation of a Single-Crystal Aluminum-Based MOF Nanowire with Graphene Oxide Nanoscrolls as Structure-Directing Agents

Mégane Muschi, Anusha Lalitha, Saad Sene, Damien Aureau, Mathieu Frégnaux, Imène Esteve, Lucie Rivier, Naseem Ramsahye, Sabine Devautour-vinot, Clémence Sicard, et al.

► **To cite this version:**

Mégane Muschi, Anusha Lalitha, Saad Sene, Damien Aureau, Mathieu Frégnaux, et al.. Formation of a Single-Crystal Aluminum-Based MOF Nanowire with Graphene Oxide Nanoscrolls as Structure-Directing Agents. *Angewandte Chemie International Edition*, 2020, 59 (26), pp.10353-10358. 10.1002/anie.202000795 . hal-03080047

HAL Id: hal-03080047

<https://hal.science/hal-03080047>

Submitted on 21 Dec 2020

HAL is a multi-disciplinary open access archive for the deposit and dissemination of scientific research documents, whether they are published or not. The documents may come from teaching and research institutions in France or abroad, or from public or private research centers.

L'archive ouverte pluridisciplinaire **HAL**, est destinée au dépôt et à la diffusion de documents scientifiques de niveau recherche, publiés ou non, émanant des établissements d'enseignement et de recherche français ou étrangers, des laboratoires publics ou privés.

Formation of Single Crystal Aluminum-based MOF Nanowire with Graphene Oxide Nanoscrolls as Structure-Directing Agents

Mégane Muschi,^[a] Anusha Lalitha,^[b] Saad Sene,^[a] Damien Aureau,^[c] Mathieu Fregnaud,^[c] Imène Esteve^[d] Lucie Rivier,^[c] Naseem Ramsahye,^[b] Sabine Devautour-Vinot,^[b] Clémence Sicard,^[c] Nicolas Menguy,^[d] Christian Serre,^[a] Guillaume Maurin,^{*,[b]} Nathalie Steunou.^{*,[c],[a]}

In memory of Prof. François Couty

Abstract: Here we propose an innovative strategy to synthesize single-crystal nanowires (NWs) of the Al^{3+} dicarboxylate MIL-69(Al) MOF by using graphene oxide nanoscrolls as structure directing agents. MIL-69(Al) NWs with an average diameter of 70 ± 20 nm and lengths up to 2 μm were found to preferentially grow along the [001] crystallographic direction. Advanced characterization tools (electron diffraction, TEM, STEM-HAADF, SEM, XPS) and molecular modelling revealed the mechanism of formation of MIL-69(Al) NWs involving size-confinement and templating effects. The formation of MIL-69(Al) seeds and the self-scroll of GO sheets followed by the anisotropic growth of MIL-69(Al) crystals are mediated by specific GO sheets/MOF interactions. This study delivers an unprecedented approach to control the design of 1D MOF nanostructures and superstructures.

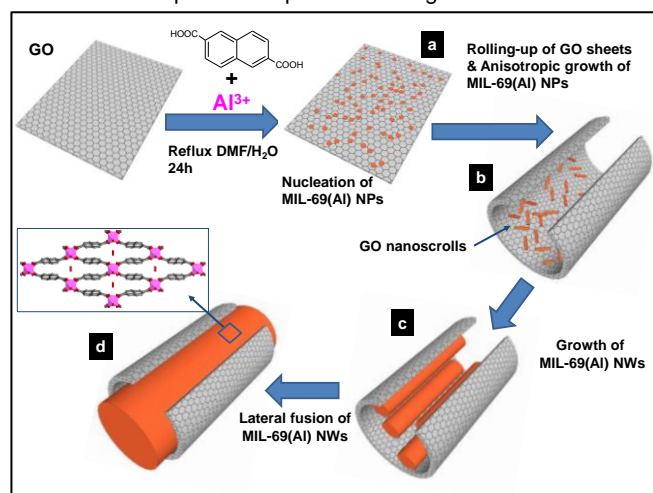
MOFs have attracted a tremendous interest over the last decades in material science since this family of porous solids offers a unique opportunity to design a wide range of architectures with modulated porosities and chemical functionality.^{1,2} These materials constructed through the assembly of metal ions and organic polydentate ligands present crystalline hybrid porous structures^{3,4} of interest for a wide range of applications including gas storage/separation, catalysis, sensing, electronics, biomedicine etc.¹ To date, most of the works on MOFs have been devoted to the discovery of novel structures, properties testing and composites processing.¹⁻¹¹ The control over the crystal size, morphology, and multi-scale porosity of MOFs as well as the shape of their crystal aggregates have been much less explored. Indeed, this was rarely achieved by using polymers, proteins, or metal oxides as additives.¹²⁻¹⁶ In particular, low-symmetry nano-crystals (NCs), which exhibit high energy facets are of interest in the fields of catalysis, sensing and electronics.^{17,18} However, only very few one-dimensional (1D) anisotropic MOF nanostructures has been discovered so far since MOF nanoparticles (NPs) are mostly

obtained as polycrystalline powders or spherical NCs.¹⁹⁻²⁴ The rare existing 1D MOF architectures in the forms of nanowires (NW), nanotubes and nanorods were synthesized through a bottom-up solution route or hydrothermal process eventually templated by polymer or inorganic 1D nanostructures.¹⁹⁻²⁴ Note that the nucleation and growth processes of 1D MOFs are far to be understood similarly to a wide range of anisotropic oxides and metal nanostructures.^{17,25,26,27} Furthermore, MOFs still present other shortcomings, which restrict their applications to a great extent. Above all, most MOFs are inherently electrically non-conductive and numerous MOFs are not robust against water/vapour or high temperature. To circumvent these drawbacks, MOF/graphene oxide (GO)-based materials⁵⁻¹¹ have attracted widespread attention in recent years since they can present an improved stability, enhanced electrical conductivity and processability as a result of a synergistic effect of the two components. These composites have been explored in various applications including sensors, supercapacitors, batteries, gas storage, and catalysis.⁵⁻¹¹ However, the development of such MOF/GO composites suffers from a disordered spatial arrangement of GO sheets and MOF particles as well as a strong aggregation of MOFs NPs. Therefore, the engineering of MOF/GO composite with hierarchical architectures, such as core-shell structure and layer-by-layer, would be most desirable to further optimize the performance of such systems.

In this context herein, we report the synthesis of single-crystal Al^{3+} dicarboxylate MOF (i.e. MIL-69(Al) MIL, Material of Institut Lavoisier) NW by using graphene oxide (GO) nanoscrolls as structure-directing agents. GO nanoscrolls are 1D carbon materials formed by rolling GO sheets from one side or from the corner into Archimedean-type spirals.²⁸ They present open structures at both ends and interlayer galleries that can be easily intercalated. Recently, the assembly of GO sheets with preformed oxide or metal NPs led to the formation of GO nanoscrolls decorated by NPs.^{28,29,30,31} Inspired by these findings, here we have exploited the potential rolling of GO to control the

- [a] Dr M. Muschi, Dr S. Sene, Dr C. Serre, Pr N. Steunou
Institut des Matériaux Poreux de Paris, UMR 8004 CNRS-ENS-ESPCI, PSL research university, Paris, France.
E-mail: nathalie.steunou@uvsq.fr
- [b] A. Lalitha, Dr N. Ramsahye, Dr S. Devautour-Vinot, Pr G. Maurin
Institut Charles Gerhardt Montpellier, UMR 5253 CNRS, Université de Montpellier, Montpellier, France.
E-mail : Guillaume.Maurin@univ-montp2.fr
- [c] Dr D. Aureau, Dr M. Fregnaud, Dr L. Rivier, Dr C. Sicard, Pr N. Steunou
Institut Lavoisier de Versailles, UMR CNRS 8180, Université de Versailles St Quentin en Yvelines, Université Paris Saclay, Versailles, France.
- [d] Dr I. Esteve, Pr N. Menguy
Sorbonne Université, UMR CNRS 7590, MNHN, IRD, Institut de Minéralogie, de Physique des Matériaux et de Cosmochimie, IMPMC, 75005 Paris, France.

Supporting information for this article is given via a link at the end of the document.



Scheme 1. Mechanistic scheme summarizing the main stages of the MIL-69(Al) NWs formation.

formation of single-crystal MOF NWs. The growth of these MOFs NWs were further scrutinized by combining multimodal *ex situ* advanced characterization techniques (electron diffraction, TEM, STEM-HAADF, SEM, XPS) and molecular modelling, thereby allowing us to propose a mechanism of formation as illustrated in scheme 1. To the best of our knowledge, this is the first study reporting the possible synthesis of single-crystal MOF NW directed by GO nan scrolls.

As a proof of concept, the microporous Al 2,6 naphthalene dicarboxylate (2,6 ndc) based MOF, denoted MIL-69(Al) was considered as a typical example.³² This network which is structurally analogue to the terephthalate-based MIL-53, is built up from the connection of infinite chains of corner-sharing octahedral $\text{AlO}_4(\text{OH})_2$ units with 2,6 ndc ligand. Its hydrated form presents one-dimensional narrow rhombic channels with a window size around $2.7 \times 13.6 \text{ \AA}$ (see scheme 1).^{33,34}

The synthesis of MIL-69(Al) NWs was conducted *in-situ* with a mixture of MOF precursors e.g. Al^{3+} salts, NaOH and 2,6 ndc and GO as a co-reactant in DMF/ H_2O solution heated under reflux. Note that the same reactants without GO led to MIL-69(Al) NPs (see SI for details).³⁵ TEM images reveal that the pure MIL-69(Al) NPs are polydisperse in size and morphology with diameters ranging from 20 to 90 nm (Figures 1(a) and S1). Varying the GO content and the heating time led to different nanostructured composites. These materials are denoted MIL-69/GO-X-Y with X and Y corresponding to the initial Al/GO weight ratio (calculated from the amount of $\text{Al}(\text{NO}_3)_3 \cdot 9\text{H}_2\text{O}$ precursor) and the reflux time respectively. The powder X-ray diffraction (PXRD) pattern of MIL-69/GO-X-24 composites displays the characteristic Bragg peaks of MIL-69(Al) in its narrow pore form, however they are much sharper and intense for X=4.5 & 9 than for X= 18 and MIL-69(Al) NPs (see Figure S2). In comparison to micrometer scale MIL-69(Al) particles, *h*00 reflections are much more intense in the PXRD pattern of MIL-69/GO-X-24, suggesting a preferential orientation of such crystals with a possible shape anisotropy. MIL-69(Al) NWs were typically obtained for X= 4.5 and after a reflux of 24 hours. As shown by N_2 porosimetry (Figure S3), MIL-69/GO-4.5-24 presents a hierarchical porous structure that consists in an

ordered array of micropores inherent of the MOF framework and mesoporous inter-particle voids. Such mesoporous voids may result from the packing of MIL-69(Al)/GO NWs or formed at the MOF/GO interfaces as previously shown for numerous MOFs based composites.^{7,14} TGA, FT-IR, Raman and XPS spectroscopies (see SI for details), revealed that this composite results from the assembling of GO and MIL-69(Al) with a GO content of 30 wt% (Figures S4-S8). Both TEM Bright field (TEM-BF) and Scanning TEM using the High Angle Annular Dark Field mode (STEM-HAADF) images evidenced that MIL-69/GO-4.5-24 is composed of inter-grown MIL-69(Al) NWs and GO sheets (Figure 1b-e). MIL-69(Al) NWs present an average diameter of $70 \pm 20 \text{ nm}$, lengths up to $2 \mu\text{m}$ and aspect ratio up to 20, as evaluated from 50 NWs randomly selected from TEM images (Figures S9-S11). Note that the morphology of MIL-69(Al) NWs is completely different than nano- or micrometer sized MIL-69(Al) particles (see Figure S1). Selected area electron diffraction (SAED) analyses were performed at low voltage (60 kV) in order to reduce the irradiation damage on a series of isolated NWs, showing the presence of single crystalline MIL-69(Al) NWs. (Figures 1f, S9-S10). To fully demonstrate that each MIL-69(Al) NW does not consist of an assembly of smaller single-crystalline particles, three SAEDs were acquired along the long axis for each NW (Figure S10). These corresponding SAED patterns clearly show that each NW corresponds to a single crystal of MIL-69(Al). From the SAED indexation, it can be inferred that each NW grows along the [001] direction which is parallel to the chain axis of the corner-sharing Al^{3+} octahedra in the structure of MIL-69(Al) (Figures S9-S10).³²

MIL-69/GO composites were also prepared with a higher Al content. MIL-69/GO-9-24 consists of bundles of MIL-69(Al) 1D tubular nanostructures interwoven with GO sheets as shown by STEM-HAADF (Figures 2 and S12). TEM and SAED experiments evidenced analogous single crystal NWs than those of MIL-69/GO-4.5-24 with a [001] growth direction. Remarkably, STEM-HAADF and SEM images show that MIL-69/GO-9-24 contains a high amount of GO nan scrolls with a diameter ranging between 70 and 100 nm (Figures 2 and S12). Note that the diameter of GO nan scrolls is close to that of MIL-69(Al) NW

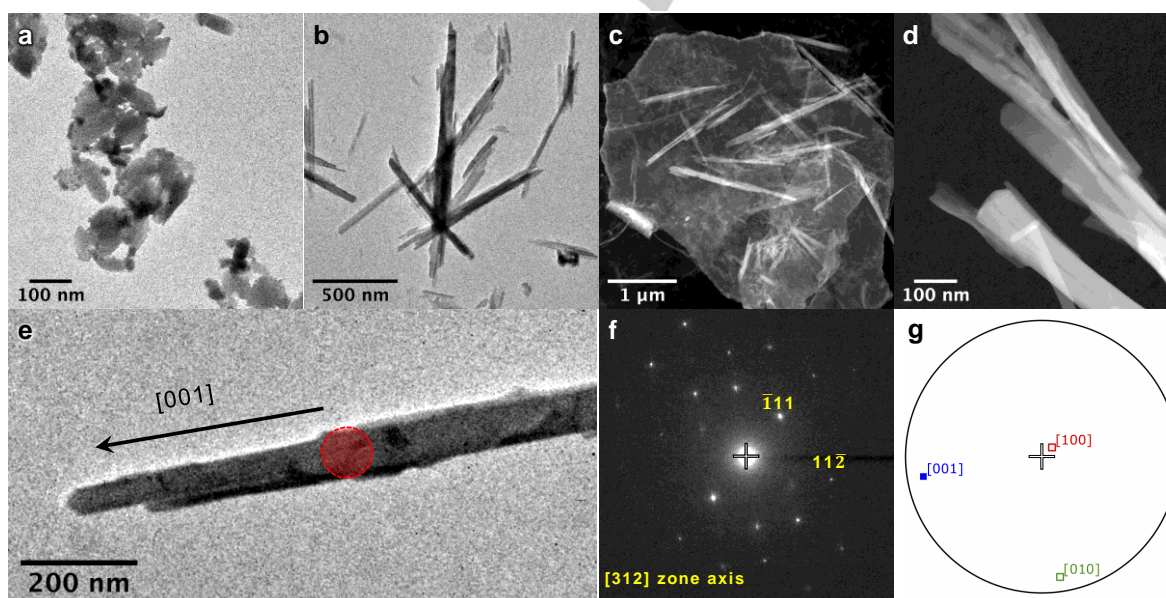


Figure 1. (a) TEM-BF image of MIL-69 NPs; (b, e) TEM-BF, (c,d) STEM-HAADF images of MIL-69/GO-4.5-24 (f) SAED of the area highlighted by the red circle in (e). The SAED indexation is given with respect to the MIL-69(Al) structure.³² The stereographic projection (g) - related to the crystallographic orientation deduced from (f) - indicates unambiguously that the crystal growth proceeds along the [001] direction (see SI for details)

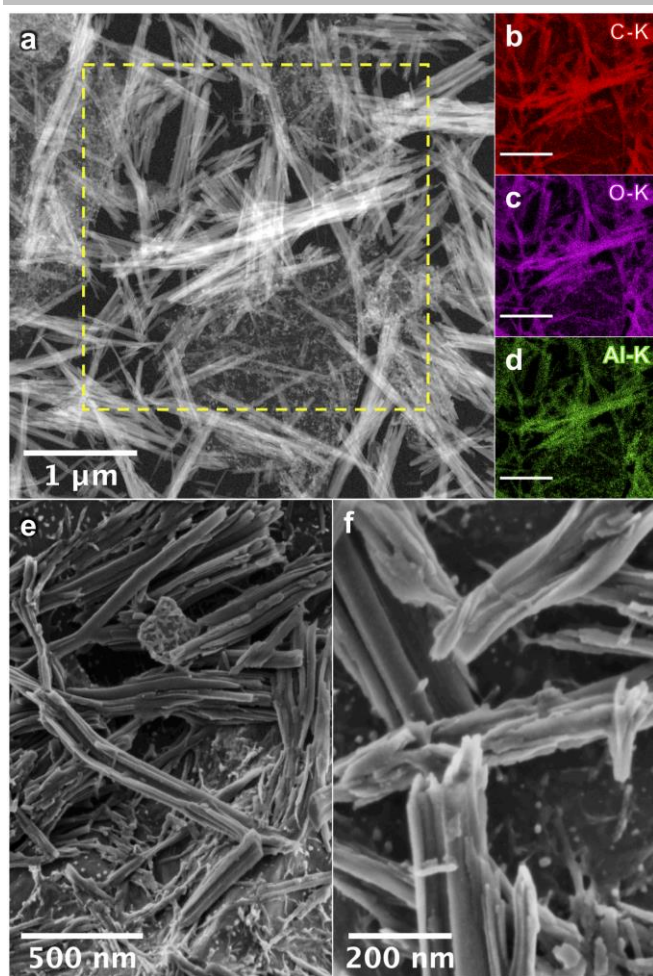


Figure 2. (a) STEM-HAADF, (b-d) STEM-XEDS elemental map for the rectangular yellow area indicated in (a), (e,f) SEM of MIL-69/GO-9-24.

suggesting a templating effect of GO. Their archimedean-type nanoscrolls morphology is reminiscent to that previously reported for maghemite/graphene composites.²⁸ Upon increasing X to 18, both TEM and STEM-HAADF images revealed the co-existence of GO sheets and bundles of 1D GO nanoscrolls. (Figure S13) with only MIL-69(Al) as NPs. This observation emphasizes that Al/GO content needs to be critically controlled to ensure the formation of MIL-69(Al) NWs.

A series of samples was collected at different stages of the reflux and further characterized by TEM, STEM-HAADF and PXRD (Figure 3 & Figures S14-S15) in order to follow the GO-assisted formation of MIL-69(Al) NWs. At this stage, MIL-69/GO-9 was considered as a model system to emphasize the interplay between the formation of GO nanoscrolls and of MIL-69(Al) NWs. After a reflux of 2 hours, the sample consists of individual GO sheets and aggregates of a few 100 nm in size (Figures 3 and S14). These aggregates result from the assembly of GO sheets and MIL-69(Al) nanoparticles as shown by PXRD and FT-IR (Figure S15). The progressive crystallization and growth of MIL-69(Al) NWs starts to be observed after a reflux of 4 hours. As shown by high resolution TEM, MIL-69(Al) NWs with a diameter of 10 nm can be observed growing along the [001] direction (Figure S14 B). For a reflux of 12 hours, bundles of almost parallel GO nanoscrolls and MIL-69(Al) NWs emerge from the aggregates (Figures 3e and S14). This suggests that

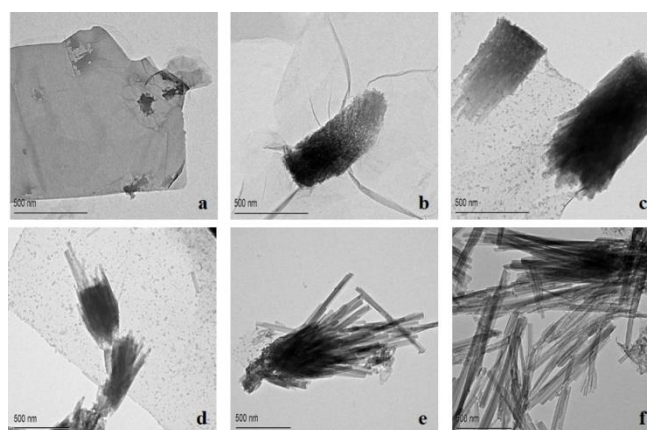


Figure 3. TEM images of MIL-69/GO-9-Y prepared with different duration Y of the reflux namely a) 1 h b) 2 h c) 4 h d) 8 h e) 12 h f) 24 h.

these aggregates act as anchors for the initial formation of MIL-69(Al) seeds, followed by their further outward growth, gradually forming the 1D GO nanoscrolls and MIL-69(Al) NWs.

An atomistic model of the interface formed between the GO sheet and the MIL-69(Al) surface was constructed and further analyzed by applying our recently developed computational strategy.^{36,37} A GO model integrating both basal functions, i.e., epoxy and hydroxyl groups and edged carboxylic acid groups, was brought into contact with two distinct 3D MIL-69(Al) slab models that represent its crystallographic (010) and (001) surfaces and the resulting composites were geometry optimized by Molecular Dynamics (MD) simulations (see SI for details). The plot of the normalized atomic density along the z axis for the optimized MIL-69(010)/GO (Figure 4a) and MIL-69(001)/GO models (Figure S21a) respectively emphasizes the formation of an interfacial zone denoted A with a z-length of 4.5 Å where the GO terminations penetrate the pore pocket of the MIL-69(Al) surfaces. This observation confirms the good affinity observed experimentally between the two components. The radial distribution functions (RDFs) plotted for diverse MOF/GO pairs evidenced (Figure 4b and Figure S23a) that the MOF/GO interactions imply the OH groups present along the chain of MIL-69(Al) and the functional groups of GO. The most prominent interaction between the edged carboxylic acid functions and the OH groups of MIL-69(Al) (Figure 4c) leads to a significant twisting of the GO-layer in direct contact with the MOF as also suggested by the analysis of the dihedral angle distribution plotted for GO (Figure S22). Such predicted high degree of distortion for the first GO layers is expected to act as a driving force for the scrolling of GO evidenced experimentally. Interestingly, the intensity of the RDF peaks for all MOF/GO pairs is four times higher for MIL-69(010)/GO (Figure 4b) than for MIL-69(001)/GO (Figure S23a). This reveals that GO more strongly interacts with MIL-69(010) than MIL-69(001). We further disclosed that GO arranges at the MIL-69(Al) (010) surface in such a way to establish π - π like-stacking interactions where the naphthalene linker lies parallel to the aromatic ring of GO (Figure 4d). Besides reinforcing the affinity between the two components, such π - π like-stacking interactions may limit the relative crystal growth of the MIL-69(010) surface. This prediction is fully consistent with the experimental observation of an anisotropic growth of MIL-69(Al) NW along the [001] direction.

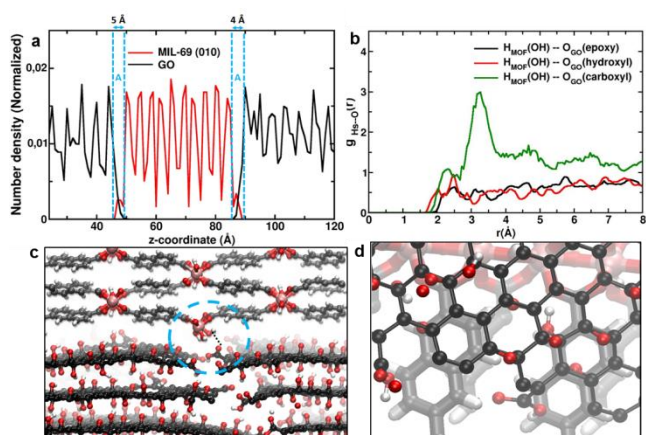


Figure 4. MIL-69(Al)(010)/GO model a) Representation of the normalized atomic density showing the interfacial region denoted A. (b) Radial Distribution Functions calculated between H_{OH} of MIL-69(Al) and the different O atoms of the functional groups of GO (c) Illustrative snapshot showing the main interactions between the edge carboxylic acid groups of GO and H_{OH} of MIL-69(Al). (d) Snapshot showing preferential π - π like interactions at the MIL-69(Al)(010)/GO interface. Color schemes are GO layers: C-black; O-red, H-white; MIL-69(010): C-gray, Al-pink, O-red and H-white.

The key role of the π - π stacking interactions through the naphthalene ring of MIL-69(Al) in the formation of NWs is also supported experimentally with the absence of NWs when we considered the *in situ* formation of the isostructural MIL-53(Al)- NH_2 in the presence of GO (see Figures S24 for more details).

The combination of *ex situ* experiments and molecular modelling not only revealed the GO-assisted formation of MIL-69(Al) NWs but also grasped a series of evidences that led us to propose the mechanism of formation summarized in Scheme 1. This is a stepwise mesoscale mechanism that involves a mutual recognition between GO and MIL-69(Al): GO directs the formation of the MOF while conversely, the MOF surface may drive the structuring of GO. The first step implies a coordination of Al^{3+} cations to both the basal plane hydroxyl groups and edged carboxylate functions of GO which is favoured by the attractive electrostatic interactions between the negatively charged GO sheets (i.e., negative zeta potential of GO in aqueous solution) and Al^{3+} cations. This most probably initiates the assembly of GO sheets and the nucleation of MIL-69(Al) NPs (Scheme 1a), as previously mentioned for the MOF-253/GO composite.³⁸ Indeed for the three MIL-69/GO-X-24 composites, the surface of GO sheets is coated by MIL-69(Al) NPs with a diameter up to 50 nm as revealed by combining STEM-HAADF and STEM-XEDS elemental mapping (Figures 2a and S12). Moreover, MIL-69(Al) nanorods up to 100 nm in length were also observed at the surface of GO for X=4.5 (Figure S11b). Molecular modelling supports an anisotropic growth of MIL-69(Al) nanostructures along the [001] direction (Scheme 1a). The following step is the rolling up of GO sheets into nanoscrolls (Scheme 1b) that is favoured by relative strong interactions between GO sheets and MIL-69(Al) surfaces. In particular, MIL-69(Al) NPs located at the edges of the bended part of GO sheets may be attracted by the inner part of GO. Moreover, the spontaneous scrolling of GO sheets can occur in the presence of DMF due to the inhomogeneous distribution of hydrophilic groups (hydroxy, epoxide and carboxylic acid) of GO

and surface tension, as previously shown.³⁹ Finally, the growth of MIL-69(Al) NWs most probably occurs in the inner part of the GO nanoscrolls (Scheme 1c) based on the electrical data recorded on the composites (see Figure S25). Indeed, despite the introduction of insulating MIL-69(Al), the semi-conducting behavior of GO is maintained for MIL69/GO-X-24. In contrast, an insulating behaviour was observed by mixing preformed MIL-69(Al) NPs with GO. These results show that the homogeneous distribution of the MOF inside the GO nanoscrolls in MIL69/GO-X-24 does not disrupt the carrier traveling through the extended conjugated network in the GO sheets and sheet-to-sheet junctions. Since the internal surface of GO nanoscrolls is decorated by numerous spatially close MIL-69(Al) nanorods and NPs, their growth and assembly are thus constrained in a confined space that may drive the crystalline growth orientation in a direction parallel to the NW axis. This mechanism can involve redissolution-crystallization steps due to the highly reversible nature of coordination bonds of the MOF network. The crystal coarsening can be thus driven by the Ostwald ripening process while the "oriented attachment" mechanism previously reported for the anisotropic growth of inorganic nanocrystals or biomineralization systems can also play a significant role. This "oriented attachment" mechanism involves spontaneous self-organization of primary adjacent particles by sharing a common crystallographic orientation, followed by their fusion into single-crystalline particles.⁴⁰ As a consequence, the growth of MIL-69(Al) nanorods may proceed from the GO surface inward, forming bundles of primary smaller aligned NWs (Figure 3e and scheme 1c) growing along the [001] direction, as shown in high resolution TEM images of Figure S14B. The lateral aggregation and crystallite fusion of these smaller NWs through "oriented attachment" mechanism can lead to one single-crystalline NW (Scheme 1d) as previously reported for anisotropic metal or oxide nanostructures.^{40,41} This last crystallization step could be explained by the spatial proximity of the primary NWs. Their constrained growth may proceed through coordination reactions with unreacted MOF precursors or grain boundary consumption at the interfaces as previously reported for MOF-74-II tubular superstructures.⁴²

In summary, GO nanoscrolls were demonstrated to act as structure-directing agents to form 1D MOF NWs. The interplay between multimodal characterization techniques and molecular modelling unravels their mechanism of formation. The self-scrolling of GO sheets and the subsequent anisotropic growth of MIL-69(Al) NWs in the inner cavity of GO nanoscrolls are driven by the covalent bonding between MIL-69(Al) NPs and the hydroxyl and carboxylic acid functions of GO that restrict the crystal growth on certain facets. This leads to the formation of hierarchical porous MOF/GO composites with a core-shell microstructure allowing homogeneous and high dispersion of MIL-69(Al) NWs in the GO matrix. Considering the chemical tunability of MOFs and the possible functionalization of GO, this strategy opens up a new avenue for fabricating hierarchical and nanostructured MOF-GO composites that might be optimal systems for different applications including separation, energy storage and sensing.⁴³ As illustrated in the case of MIL-69(Al)/GO composites, the design of core-shell MOF-GO nanostructures appears as a valuable approach to integrate MOFs into GO without any agglomeration of MOFs NPs or

restacked GO layers while imparting electron transport properties. Typically, such composites combining a hierarchical porous structure in synergy with electrical conductivity might facilitate the current and electrolyte transport efficiency. This will be exploited in future work for possible applications in the field of batteries, supercapacitors and electrochemical sensors.

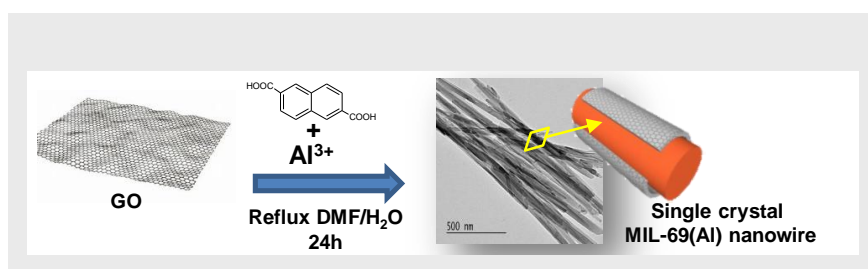
Acknowledgements

The authors would like to acknowledge the European Community Horizon 2020 Program (H2020/2014-2020) for funding the research presented in this article under Grant Agreement No. 727619 (project Gramofon). The authors would like to acknowledge B. Alonso, A. Ortega from Graphenea S. A. (www.graphenea.com) for providing the graphene oxide sample. N. Heymans and G. De Weireld (University of Mons) are acknowledged for useful discussions. NM is grateful to Dr Jean-Michel Guigner (IMPIC) for JEOL LaB6 TEM settings at 60 kV. NS would like to thank Dr Effrosyni Gkaniatsou for SEM measurements on MIL-69(Al) microparticles.

Keywords: metal-organic frameworks • graphene oxide • nanowire • self-assembly • template

- [1] P. K. Bharadwaj, P. Feng, S. Kaskel, Q. Xu, *Chem. Asian J.* **2019**, *14*, 3450–3451.
- [2] D. Zhao, P. K. Thallapally, C. Petit, J. Gascon, *ACS Sustainable Chem. Eng.* **2019**, *7*, 7997–7998.
- [3] M. O’Keeffe, O. M. Yaghi, *Chem. Rev.* **2012**, *112*, 675–702.
- [4] J. Cepeda, S. Perez-Yanez, G. Beobide, O. Castillo, E. Goikolea, F. Aguesse, L. Garrido, A. Luque, P.A. Wright, P. A. *Chem. Mater.* **2016**, *28*, 2519–2528.
- [5] A. Huang, Q. Liu, N. Wang, Y. Zhu, J. Caro, *J. Am. Chem. Soc.* **2014**, *136*, 42, 14686–14689.
- [6] Y. Hu, J. Wei, Y. Liang, H. Zhang, X. Zhang, W. Shen, H. Wang, *Angew. Chem. Int. Ed.* **2016**, *55*, 2048–2052.
- [7] D. Kim, D. Woo Kim, W. G. Hong, A. Coskun, *J. Mater. Chem. A* **2016**, *4*, 7710–7717.
- [8] J. Wang, Y. Wang, Y. Zhang, A. Uliana, J. Zhu, J. Liu, B. Van der Bruggen, *ACS Appl. Mater. Interfaces* **2016**, *8*, 25508–25519.
- [9] J. Wei, Y. Hu, Y. Liang, B. Kong, Z. Zheng, J. Zhang, S. Ping Jiang, Y. Zhao, H. Wang, *J. Mater. Chem. A* **2017**, *5*, 10182–10189.
- [10] M. Muschi, C. Serre, *Coord. Chem. Rev.* **2019**, *387*, 262–272.
- [11] Y. Hu, Y. Wu, C. Devendran, J. Wei, Y. Liang, M. Matsukata, W. Shen, A. Neild, H. Huang, H. Wang, *J. Mater. Chem. A* **2017**, *5*, 16255–16262.
- [12] M. Pang, A. J. Cairns, Y. Liu, Y. Belmabkhout, H. C. Zeng, M. Eddaoudi, *J. Am. Chem. Soc.* **2013**, *135*, 10234–10237.
- [13] J. Huo, M. Marcelllo, A. Garai, D. Bradshaw, *Adv. Mater.* **2013**, *25*, 2717–2722.
- [14] D. Bradshaw, S. El-Hankari, L. Lupica-Spagnolo, *Chem. Soc. Rev.* **2014**, *43*, 5431–5443.
- [15] J. Hwang, T. Heil, M. Antonietti, B. V. K. J. Schmidt, *J. Am. Chem. Soc.* **2018**, *140*, 2947–2956.
- [16] S. Jr. Ayala, K. C. Bentz, S. M. Cohen, *Chem. Sci.* **2019**, *10*, 1746–1753.
- [17] L. Pan, P. Gao, E. Tervoort, A. M. Tartakovsky, M. Niederberger, *J. Mater. Chem. A* **2018**, *6*, 18551–18560.
- [18] N. Steunou, J. Livage, *CrystEngComm* **2015**, *17*, 6780–6795.
- [19] M. Jahan, Q. Bao, J. –X. Yang, K. P. Loh, *J. Am. Chem. Soc.* **2010**, *132*, 14487–14495.
- [20] X. Dao, Y. Ni, *Dalton Trans.* **2017**, *46*, 5373–5383.
- [21] R. C. Arbulu, Y.-B. Jiang, E. J. Peterson, Y. Qin, *Angew. Chem. Int. Ed.* **2018**, *57*, 5813–5817.
- [22] L. Zou, C.-C. Hou, Z. Liu, H. Pang, Q. Xu, *J. Am. Chem. Soc.* **2018**, *140*, 15393–15401.
- [23] T. He, S. Chen, B. Ni, Y. Gong, Z. Wu, L. Song, L. Gu, W. Hu, X. Wang, *Angew. Chem. Int. Ed.* **2018**, *57*, 3493–3498.
- [24] J. Shi, J. Zhang, D. Tan, X. Cheng, X. Tan, B. Zhang, B. Han, L. Liu, F. Zhang, M. Liu, J. Xiang, *ChemCatChem* **2019**, *11*, 2058–2062.
- [25] G. T. Chandrappa, N. Steunou, S. Cassaignon, C. Bauvais, J. Livage, *J. Catal. Today* **2003**, *78*, 85–89.
- [26] M. Jaber, F. Ribot, L. Binet, V. Briois, S. Cassaignon, K. J. Rao, J. Livage, N. Steunou, *J. Phys. Chem. C* **2012**, *116*, 25126–25136.
- [27] R. Deshmukh, M. Niederberger, *Chem. Eur. J.* **2017**, *23*, 8542–8570.
- [28] T. Sharifi, E. Gracia-Espino, H. Reza Barzegar, X. Jia, F. Nitze, G. Hu, P. Nordblad, C.-W. Tai, T. Wägberg, *Nature Comm.* **2013**, *4*, 2319.
- [29] H. Pang, Q. Lu, F. Gao, *Chem. Commun.* **2011**, *47*, 11772–11774.
- [30] X. Wang, D.-P. Yang, G. Huang, P. Huang, G. Shen, S. Guo, Y. Mei, D. Cui, *J. Mater. Chem.* **2012**, *22*, 17441–17444.
- [31] M. Yan, F. Wang, C. Han, X. Ma, X. Xu, Q. An, L. Xu, C. Niu, Y. Zhao, X. Tian, P. Hu, H. Wu, L. Mai, *J. Am. Chem. Soc.* **2013**, *135*, 18176–18182.
- [32] T. Loiseau, C. Mellot-Draznieks, H. Muguerra, G. Férey, M. Haouas, F. Taulelle, *C. R. Chim.* **2005**, *8*, 765–772.
- [33] I. Senkowska, F. Hoffmann, M. Fröba, J. Getzschmann, W. Böhlmann, S. Kaskel, *Micropor. Mesopor. Mater.* **2009**, *122*, 93–98.
- [34] P. L. Feng, K. Leong, M. D. Allendorf, *Dalton Trans.* **2012**, *41*, 8869–8877.
- [35] A. Sabetghadam, X. Liu, M. Benzaqui, E. Gkaniatsou, A. Orsi, M. M. Lozinska, C. Sicard, T. Johnson, N. Steunou, P. A. Wright, C. Serre, J. Gascon, F. Kapteijn, *Chem. Eur. J.* **2018**, *24*, 7949–7956.
- [36] R. Semino, N. A. Ramsahye, A. Ghoufi, G. Maurin *ACS Appl. Mater. Interfaces* **2016**, *8*, 809–819.
- [37] S. Bonakala, A. Lalitha, J. E. Shin, F. Moghadam, R. Semino, H. B. Park, G. Maurin, *ACS Appl. Mater. Interfaces* **2018**, *10*, 33619–33629.
- [38] X. Qiu, X. Wang, Y. Li, *Chem. Commun.* **2015**, *51*, 3874–3877.
- [39] B. Tang, Z. Xiong, X. Yun, X. Wang, *Nanoscale* **2018**, *10*, 4113–4122.
- [40] a) R. L. Penn, J. F. Banfield, *Science*, **1998**, *281*, 969–971; b) J. F. Banfield, S. A. Welch, H. Zhang, T. Thomsen Elbert, *Science*, **2000**, *289*, 751–754; c) D. Li, M. H. Nielsen, J. R. J. Lee, C. Frandsen, J. F. Banfield, J. J. De Yoreo, *Science*, **2012**, *336*, 1014–1018; d) Q. Zhang, S.–J. Liu, S.–H. Yu, *J. Mater. Chem.* **2009**, *19*, 191–207.
- [41] M. Li, F. Kong, H. Wang, G. Li, *CrystEngComm* **2011**, *13*, 5317–5320.
- [42] L. Feng, J. –L. Li, G. S. Day, X. –L. Lv, H. –C. Zhou, *Chem*, **2019**, *5*, 1–10.
- [43] a) Y. Zheng, S. Zheng, H. Xue, H. Pang, *Adv. Funct. Mater.* **2018**, *28*, 1804950; b) H. Wu, W. Zhang, S. Kandambeth, O. Shekhan, M. Eddaoudi, H. N. Alshareef, *Adv. Energy Mater.* **2019**, *9*, 1900482.

COMMUNICATION



Dr Mégane Muschi, Anusha Lalitha, Dr Saad Sene, Dr Damien Aureau, Dr Mathieu Fregnaud, Dr Imène Esteve, Dr Lucie Rivier, Dr Naseem Ramsahye, Dr Sabine Devautour-Vinot, Dr Clémence Sicard, Prof. Nicolas Menguy, Dr Christian Serre, Prof. Guillaume Maurin, Prof. Nathalie Steunou.**

Page No. – Page No.

Title

Single-crystal nanowires (NWs) of the Al^{3+} dicarboxylate MIL-69(Al) MOF were synthesized by using graphene oxide nanoscrolls as structure directing agents. The interplay between multimodal characterization techniques and molecular modelling unravels their mechanism of formation involving size-confinement and specific interactions.